HHS Public Access

Author manuscript

J Phys Chem B. Author manuscript; available in PMC 2019 February 08.

Published in final edited form as:

J Phys Chem B. 2018 February 08; 122(5): 1600–1607. doi:10.1021/acs.jpcb.7b11352.

Multi-Funnel Landscape of the Fold-Switching Protein RfaH-CTD

Nathan A. Bernhardt and **Ulrich H. E. Hansmann**

Dept. of Chemistry & Biochemistry, University of Oklahoma, Norman, OK 73019, USA

Abstract

Proteins such as the transcription factor RfaH can change biological function by switching between distinct three-dimensional folds. RfaH regulates transcription if the C-terminal domain folds into a double helix bundle, and promotes translation when this domain assumes a β-barrel form. This fold-switch has been also observed for the isolated domain, dubbed by us RfaH-CTD, and is studied here with a variant of the RET approach recently introduced by us. We use the enhanced sampling properties of this technique to map the free energy landscape of RfaH-CTD and to propose a mechanism for the conversion process.

TOC Graphic

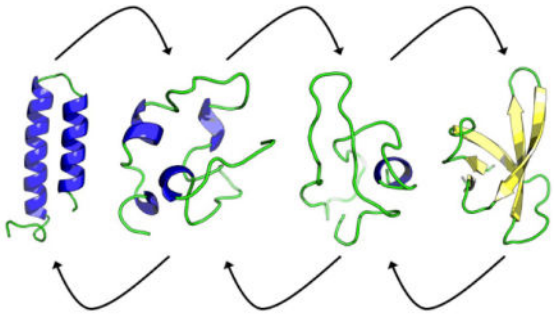

Introduction

Proteins play a central role in the biochemistry of cells, participating in transcription, cell signaling, migration and muscle movement to name only a few of their roles. Protein function is correlated with the molecule assuming a specific three-dimensional shape, but the process by that a protein folds into a certain structure is not known in all details, and depends not only on the sequence of amino acids (the chemical composition of a protein) but also on environment and interaction with other molecules. In the standard model of protein folding, one assumes that a protein has a funnel-shaped energy landscape[1,2] that guides a multitude of possible folding pathways into a unique structure where the protein is biologically active. However, such a single-funnel picture cannot describe all aspects of

Correspondence to: Nathan A. Bernhardt; Ulrich H. E. Hansmann.

Supporting Information

A pdf-file containing supplemental figure S1 (convergence of simulation) and supplemental table S1 (acceptance rates for exchange moves).

folding for all proteins. For instance, intrinsically disordered proteins[3–5] do not have a defined structure, but may assume one when interacting with other proteins, with the structure changing with the binding partner. In other cases, proteins exist in an ensemble of different (but defined) structures[6–8] which may allow proteins to have more than one function in the cell. In these cases we would expect a multi-funnel shaped folding landscape.

Take as an example RfaH,[9] a protein that triggers gene expression in Escherichia coli by switching the structure of the C-terminal domain from an α-helical hairpin (PDB-ID: 2OUG) to a β-barrel (PDB-ID: 2LCL), see Figure 1. In the first form, stabilized by interaction with the N-terminus, the C-terminal domain masks a RNA polymerase binding site on the N-terminal domain thus regulating transcription. However, when not in contact with the N-terminal domain, or as an isolated protein, the C-terminal domain spontaneously rearranges into a β-barrel (Figure 1). In this form, RfaH binds directly to the ribosomal protein S10, thus recruiting the prokaryotic ribosomal 30S subunit to the elongating RNA and promoting translation. Hence, the fold switch of the C-terminal domain alters dramatically the function of the RfaH protein. Both folds are encoded in the sequence of the C-terminal domain, and it is the interaction (or lack of interaction) with the N-terminus of RfaH that selects the fold. Hence, we would expect a double-funneled landscape for the isolated 66-residue large C-terminal domain of RfaH (RfaH-CDT), with one funnel leading to the β-barrel, and the secondary funnel leading to the α-helical hairpin.[10] The rather small size, the experimentally observed fold switching, and the resolved structures of the two folds make RfaH-CTD an ideal model to study the factors that determine protein plasticity and the mechanism of fold switching in proteins.

However, probing such fold switching and mapping their energy landscape by experiments or *in silico* is a challenge.[10–14] Computationally, the problem is that the exploration of the ensemble of possible structures and the conversion between these structures happens on timescales that, on general-purpose computers, are not accessible in all-atom molecular dynamics simulations with explicit solvent. Enhanced sampling techniques such as Replica Exchange Molecular Dynamics (REMD)[15–20] promise to overcome this problem by realizing a random walk in temperature which allows the system to escape out of traps and cross barriers by explorations to higher temperatures. However, the sampling efficiency of REMD is often below the theoretical maximum. One problem is that the probability for a replica exchange depends on the temperature spacing which shrinks dramatically with system size. Hence, with the inclusion of water molecules one needs even for small proteins a huge number of replica. This often makes REMD simulations of proteins with explicit solvent impractical, and previous REMD simulations of RfaH[11] had for this reason to rely on an implicit solvent. While these simulations allowed the authors to propose a transition pathway between the two folds, choice of an implicit solvent is not without problems. While the helix-hairpin was found, the simulation was unable to completely fold the β-barrel. Only when continuing the simulations from the best configurations by including solvent molecules explicitly was the correct β-barrel fold found.[11]

We have recently proposed to overcome some of the limitations that hold back REMD by a Replica-Exchange-with-Tunneling (RET) approach.[21] We have shown that RET in conjunction with a Hamilton-Replica-Exchange[22,23] of systems where the “physical” system

is coupled to varying degrees with biasing Go-models, allows efficient simulation of proteins and protein assemblies that can take more than one state.[24,25] For instance, we have used this approach in a a recent study[24] of the two mutants GA98 and GB98, which differ only in a single residue but keep the distinct original folds of the A and B domain of protein G, GA and GB.[26–28] We have shown how the mutation leading from GA98 to GB98 alters the energy landscape leading to selection of one fold over the other.[24] While there exist alternative techniques, for instance, double-Lorentzian restraints,[29] to enhance transitions between configurations, we use in the present work the above discussed approach, with which we are more familiar, to explore the folding and switching landscape of the C-terminal domain of RfaH, Rfah-CTD, and propose a conversion process that connects the two forms.

Materials and Methods

When simulating conformational transitions in systems with competing attractors as in the case of RfaH-CDT (an α-helical hairpin and a β-barrel), one way to enhance transitions between the two attractors is to utilize exchange moves between "physical" models and such relying on Go-type force fields that bias toward one or the other of the competing configurational states. Go-models are defined by energy functions that depend directly on the similarity to a pre-selected structure, and therefore lead to a smooth energy landscapes with a single funnel located around the target fold. As a consequence, Go models fold proteins quickly, but are by construction unable to capture accurately the energetics of non-native folds. Thus, in an effort to exploit the quick folding of Go models but remove the associated bias against non-native folds, one can design a Hamilton Replica Exchange Method[22] where at each replica a "physical" model is "fed" by a Go-model, but where the bias differs for each replica.[25,30,31] In the present implementation, the physical and the Go-model are coupled through a potential that depends on the similarity between configurations in the two models[31,32]

$$E_\lambda = \begin{cases} \frac{1}{2}\left(\Delta^2(i,j)\right) & -ds < \Delta(i,j) < ds \\ A + \frac{B}{\Delta^S(i,j)} + f_{max}\Delta(i,j) & \Delta(i,j) > ds \\ A + \frac{B}{\Delta^S(i,j)}(-1)^S - f_{max}\Delta(i,j) & \Delta(i,j) < -ds \end{cases} \quad (1)$$

such that $\Delta(i, j)$ is the difference in distances between alpha carbons i and j in the respective models, f_{max} is a parameter that controls the maximum force as $\Delta(i, j) \rightarrow \infty$, and S controls how fast this value is reached. The parameters A and B are set so that the potential and its first derivative are continuous at values of $\Delta(i, j) = \pm ds$, and are expressed as

$$A = \left(\frac{1}{2} + \frac{1}{S}\right) ds^2 - \left(\frac{1}{S} + 1\right) f_{max} ds \quad and \quad B = \left(\frac{f_{max} - ds}{S}\right) ds^{S+1} \quad (2)$$

Thus the total potential energy of the system is

$$E_{pot}=E_{phy}+E_{go}+\lambda E_{\lambda} \quad (3)$$

where λ controls how strongly the physical and Go-models are coupled. Hamilton Replica Exchange now introduces a random walk in λ-space, with data to be analyzed only from the replica where the bias from the Go-model on the physical model vanishes, i.e., λ = 0.

However, exchange rates are often low in such an approach. This is a common problem in replica-exchange sampling[15,16,18] which in its standard implementation aims to enforce a random walk in temperature as a way to escape out of local minima in order to achieve faster convergence at a (low) target temperature. Unfortunately, the exchange move between neighboring temperatures often leads to a proposal state that is exponentially suppressed, but if accepted the multiple replica system quickly relaxes to a state of comparable probability to that before the exchange. As a way to overcome this bottleneck and tunnel through the unfavorable transition we have recently introduced Replica-Exchange-with-Tunneling (RET)[21,24,25] by the following four-step-procedure:

1. In the first step, the configurations $A(B)$ evolve on two neighboring replica over a short microcanonical molecular dynamics trajectory to configurations $A'(B')$, without that the total energies E_1 and E_2 change on the two replicas. However, there will be an exchange between potential and kinetic energy on each replica.
2. Next, the configurations A' and B' are exchanged, and the velocities are rescaled according to the following equations such that the energies remains constant before and after the exchange: $E_1^{'}=E_1$ and $E_2^{'}=E_2$.

$$v_A^{''}=v_A^{'}\sqrt{\frac{E_2-E_{pot}(q_A^{'})}{E_{kin}(v_A^{'})}} \quad \text{and} \quad v_B^{''}=v_B^{'}\sqrt{\frac{E_1-E_{pot}(q_B^{'})}{E_{kin}(v_B^{'})}} \quad (4)$$

3. After the exchange, the two replica evolve again by microcanonical molecular dynamics. While the total energies E_1 and E_2 on the two replica do not change, the exchange between potential and kinetic energy will lead to final states B' on replica 1 and A' on replica 2 that have potential energies comparable to the corresponding configurations before the exchange move, and velocity distributions as one would expect for the given temperatures at each replica.
4. The final configurations on each replica are either accepted or rejected according to the following Metropolis criterion

$$\exp\left(-\beta_1(E_{pot}(\hat{q}_B)-E_{pot}(q_A))-\beta_2(E_{pot}(\hat{q}_A)-E_{pot}(q_B))\right) \quad \text{with} \quad \beta=1/k_BT. \quad (5)$$

If rejected, molecular dynamics simulations continue with the original configurations $A(B)$. However, in both cases, new velocity distributions are randomly drawn according to the temperatures on the respective replica.

For more details on this approach and its limitations, see Refs.[21,24]

In the present study we use RET moves to overcome the problem of low exchange rates in our above described set-up. Velocities are rescaled according to

$$v''_A = v'_A \sqrt{\frac{E_2 - E_{phys}(q'_A) - E_{Go}(q'_A) - \lambda_2 E_\lambda(q'_A)}{E_{kin}(v'_A)}}$$
$$v''_B = v'_B \sqrt{\frac{E_1 - E_{phys}(q'_B) - E_{Go}(q'_B) - \lambda_1 E_\lambda(q'_B)}{E_{kin}(v'_B)}}, \quad (6)$$

and RET moves are accepted with probability

$$\exp\left(-\beta_1\left(\Delta E^{(1)}_{phys} + \Delta E^{(1)}_{go} + \lambda_1 \Delta E^{(1)}_{\lambda}\right) - \beta_2\left(\Delta E^{(2)}_{phys} + \Delta E^{(2)}_{go} + \lambda_2 \Delta E^{(2)}_{\lambda}\right)\right) \quad (7)$$

where $\Delta E^{(1)}_{phys} = E_{phys}(\hat{q}_B) - E_{phys}(q_A)$ and $\Delta E^{(2)}_{phys} = E_{phys}(\hat{q}_A) - E_{phys}(q_B)$; $\Delta E^{(i)}_{Go}$ and $\Delta E^{(i)}_{\lambda}$ are defined accordingly.

In the present example we have two ladders of replica, each covering a range from $\lambda = 0$ to a value $\lambda = \lambda_{max}$. In the one ladder, replicas walk between a system with no bias on the physical model to one where there is maximal bias toward the α-helix hairpin; in the other the biasing is toward the β-barrel. The two $\lambda = 0$ replica do not exchange configurations but serve as reservoirs from that a canonical simulation at the same temperature is “fed” by a heat bath move.

We consider in our simulations not the full-length RfaH protein but only the 48-residue-long C-terminal domain, RfaH-CTD. The RfaH-CTD protein is capped at the N-terminus by an acetyl group, and by a methylamine group at the C-terminus. Prior to running large scale simulations initial structures were randomized by high temperature molecular dynamics (T = 3500 K). Replicas were then brought to their initial lambda values in a short preproduction run. A total of 25 replicas with a lambda distribution of λ = 0.4, 0.2, 0.1, 0.075, 0.055, 0.035, 0.028, 0.023, 0.015, 0.010, 0.005, 0.00, 0.00, 0.00, 0.005, 0.010, 0.015, 0.023, 0.028, 0.035, 0.055, 0.075, 0.1, 0.2 and 0.4 is used. The E_λ energy function of Eq. 1 is parametrized with ds = 0.3Å, S = 1 and f_{max} = 0. Data were generated over 100 ns trajectories using an in house version of GROMACS 4.6.5[33] (available from the authors on request), modified to accommodate RET sampling and the Go-model feeding. Potential energy calculations relied on the CHARM36 force field[34] in combination with a GBSA implicit solvent[35] for the physical model and the smog energy function[36,37] for the Go-

model (using the online SMOG server at http://smog-server.org). Equations of motion are integrated by a leap frog integrator with a time step of 2 fs, which requires use of the linear constraint solver (LINCS)[38] for constraining hydrogen and heavy atom bond distances. A plain cutoff of 1.5 nm was used for treatment of electrostatics, and the v-rescale thermostat[39] is used to keep the temperature at 310 K.

Results and Discussions

We start our analysis by first testing that our simulations have converged. For this purpose, we have calculated the later discussed free energy landscape for different intervals of the 100 ns trajectory, see Figure S1 in the Supplemental Informations. Comparing these landscapes we see that our trajectory has converged after 30 ns, and therefore use the last 70 ns for our analysis. Within this time interval, we observe an average exchange rate between neighboring replicas, with individual rates listed in table S1, of 26 ± 3%, a value that is similar to the one seen by us in previous RET simulations where we also showed that regular Hamilton Exchange Replica Exchange let to lower rates (especially around $\lambda = 0$) if the same number of replica is used.[21,24,25] As a consequence, replica can walk on both sides of the ladder between replica with $\lambda = \lambda_{max}$ where the physical model is biased strongly by the corresponding Go-model, and $\lambda = 0$ where the physical model is not biased by the Go-model. The number of walks between the two extreme values (called by us tunneling events) are a measure for the quality of simulation. In the present study, we observe a total of 34 tunneling events, with examples shown in Figure 2, a value that in our previous work indicated that our simulations had sampled sufficient statistics. We remark that we saw in previous simulations[21,24,25] always much higher numbers of tunneling events when using RET exchange moves than in regular Hamilton Exchange Replica Exchange with the same number of replicas and the same λ distribution, reflecting the superior sampling that results from the RET move.

Note that the observed tunneling events cannot be interpreted as folding events leading to either the helix-hairpin or the β-barrel state as our RET simulations rely on an artificial dynamics. This is a common problem in all generalized-ensemble and replica-exchange simulations, but one that can be circumvented by reconstructing the free energy landscape of the system under consideration. We show in Figure 3 this landscape projected on the root-mean-square-deviation to either the helix hairpin structure (x-axis) or the β-barrel (y-axis). Bin sizes were chosen as 0.8 angstroms, a value smaller than the maximal root-mean-square deviation between models of the 2LCL NMR ensemble, and the landscape was smoothen to interpolate between bins. Note, that this landscape is derived only from the unbiased replica, i.e. the one that has no contribution from a Go-term but is “fed” by the two sides of the ladder of replica, on one side is the physical model biased by the Go-term with varying degrees toward the helix-hairpin, and on the other side is the bias is toward the β-barrel.

Besides the landscape we show also in Figure 3 representative structures for the various regions, labeled A to I. Visual inspection and clustering analysis[40] of the landscape indicates that the β-barrel state (region H and I) is the preferred fold of RfaH-CTD, with about 21% of all configurations in the β-barrel form. However, the bound state state (region A and B) is also significantly populated, with roughly 6% of configurations in the helix hairpin state.

Both folds differ by only approximately 2 RT in free energy, but are separated by a barrier of at least 10 RT. The majority of sampled configurations, 73 %, are either disordered or not representative of either fold. Visual inspection of the free energy landscape in Figure 3 suggests that the transition between helix-hairpin and β-barrel state might involve a disordered crossover state, see the chain of arrows in the landscape used to trace a possible transition pathway.

Moving from the region of fully-formed helix hairpin (A), helix 2 of RfaH-CTD begins to deteriorate as seen by visual inspection of the configurations in region (B). Moving further along this region, helix 1 begins also to dissolve. Moving out of this basin requires to dissolve the backbone hydrogen bonds that stabilize the two helices, leading to a free energy barrier of about 10 RT, see region C. This is supported by the hydrogen-bond analysis in Figure 4 where we define a hydrogen bond by donor acceptor distances of less than 3.5 angstroms and an &*agr;* angle of less than 30°.

Upon crossing the barrier (C), the RfaH-CTD molecule moves through an ensemble of disordered configurations with little or no defined secondary structure. However in this region (D), β-hairpins begin to form in what appears to be a random fashion, and eventually, after crossing a much smaller barrier (E) of about 4 RT, a stable hairpin between β3 and β4 forms in region F. At this point β1 has also begun to make contacts with β2. Upon entering region G, β2 starts to attach to β3 of the β-hairpin structure, bringing β1 with it. Interestingly, there exists a small helix, stabilized by several hydrogen bonds, in the linker region connecting β1 and β2. This helix positions β1 higher up than in the ideal fold likely making it difficult for β5 to lay on top of it. Only after finally crossing a third much smaller barrier of less than 2 RT, possibly due to loss of hydrogen bonds in the small helix between β1 and β2, does RfaH-CTD start to assume in region H the β-barrel form. Surprisingly the contacts between β5 and β4 are maintained in this step where the upper portion of β4 bends down slightly allowing β5 to lay on top of β1 but facing in the wrong direction. In the final step, β5 works its way around the N-terminus, thus completing the β-barrel (I). This chain of events is again supported by the hydrogen bond analysis of Figure 4. Note that this chain of events is also observed in the tunneling events that we show in Figure 5. While such tunneling events do not necessarily represent “true” transition paths (as they rely on an artificial dynamics), they are added here for illustration.

The above conversion process is similar to the one proposed in previous work[11] that relied on regular REMD simulations. One difference is that in this earlier work, helix 1 breaks first as opposed to our simulations where helix 2 is the one that starts dissolving first. However, in the earlier work, a transition pathway was obtained by following a single replica moving through temperature space. As at high temperatures a replica can cross barriers insurmountable at low temperatures, the observed transition pathways result from an artificial dynamics and do not necessarily describe the correct paths. On the other hand, our scenario follows from interpreting the free energy landscape of the protein, not from observed trajectories (which would also result from an artificial dynamics and therefore not necessarily describing the correct pathway). In addition, our scenario is also supported by a comparison of the root-mean-square-fluctuation (RMSF) of residues at the two termini. The C-terminus of RfaH-CTD has a large tail consisting of seven residues following helix 2,

while at the N-terminus only three residues precede helix 1. The RMSF values in Figure 6 indicate that the larger tail at the C-terminus is much more flexible than the short end at the N-terminus whose three residues are stabilized by hydrogen bonds with residues 5 and 39 of helix 1 and helix 2. The increased mobility of the seven C-terminal residues adds extra strain on helix 2, thus disrupting its hydrogen bond pattern as is seen in Figure 4, and from visual inspection of clustering data for region (B). Note that this interpretation would not apply to the full-size RfaH protein (instead of only the C-terminal domain RfaH-CTD) which has a much larger linker region preceding helix 1.

The differences are much smaller in the remaining parts of the conversion process. Previous work also found that dissolution of the helices is followed by a disordered interconnecting state which precedes formation of a β-hairpin between β3 and β4 and then addition of β2. The strand β1 was suggested to take longer to align with the developing β-sheet due to a larger linker region but once formed would provide a template for addition of β5, thus completely folding the barrel. This order of β-sheet formation is the same as in our scenario, with the caveat that in our picture the process appears to be more dynamic: β-strands continue to grow and re-arrange as additional strands attach to the initial β-hairpin, as seen in the panels C–E of Figure 4, and become fully-formed only late in the folding pathway toward the β-barrel.

Conclusions

Using a variant of Replica-Exchange-with-Tunneling (RET) we have studied the fold switching process of the 66-residue C-domain RfaH-CTD of the transcription factor RfaH. Our enhanced sampling method allows us to calculate the free energy landscape of the protein projected on suitable coordinates. Analyzing this landscape we propose a mechanism for the conversion process between the helix-hairpin form seen when RfaH-CTD is bound to the he N-terminal domain of RfaH and blocks transcription, and the β-barrel form seen in the unbound RfaH-CTD which promotes translation. Consistent with experiments we find that the β-barrel is the preferred fold for the isolated RfaH-CTD. However, its free energy is only marginally lower than the helix-hairpin seen in the bound RfAH, but both folds are separated by large barriers resulting from the main chain hydrogen bonds of the helix hairpin. Upon dissolution of the helix hairpin, RfaH-CTD evolves into a disordered state, before a β-hairpin forms between β3 and β4. Later β2 attaches to β3 of this hairpin, with β1 being in contact already with β2. In the final steps, β4 bends slightly trapping temporarily β5 on top of β1 before this strand rearranges and completes the β-barrel fold. While the overall pathway is similar to earlier work using traditional REMD simulations[11] , our improved sampling method adds important detail, showing a less structured conversion process with secondary structure only forming late in the process. Together with our earlier work, these results establish the usefulness of our approach for studying switching proteins. We intend now to use our simulation protocol for the simulation of larger switching proteins such as the 93-residue lymphotactin[7] that would be difficult to study with regular REMD.

Supplementary Material

Refer to Web version on PubMed Central for supplementary material.

Acknowledgments

The simulations in this work were done using the SCHOONER cluster of the University of Oklahoma and XSEDE resources allocated under grant MCB160005 (National Science Foundation). We acknowledge financial support from the National Science Foundation under grant CHE1266256 and the National Institutes of Health under grant GM120578 and GM120634.

References

1. Onuchic JN, Wolynes PG. Theory of Protein Folding. Curr Opin Struc Biol. 2004; 14:70–5.
2. Leopold PE, Montal M, Onuchic JN. Protein Folding Funnels: A Kinetic Approach to the Sequence-structure Relationship. Proc Natl Acad Sci (USA). 1992; 89:8721–5. [PubMed: 1528885]
3. Dunker AK, Silman I, Uversky VN, Sussman JL. Function and Structure of Inherently Disordered Proteins. Curr Opin Struct Biol. 2008; 18:756–64. [PubMed: 18952168]
4. Dunker AK, Lawson JD, Brown CJ, Williams RM, Romero P, Oh JS, Oldfield CJ, Campen AM, Ratliff CM, Hipps KW, et al. Intrinsically Disordered Protein. J Mol Graph Model. 2001; 19:26–59. [PubMed: 11381529]
5. Dyson HJ, Wright PE. Intrinsically Unstructured Proteins and Their Functions. Nat Rev Mol Cell Biol. 2005; 6:197–208. [PubMed: 15738986]
6. Mohanty S, Meinke JH, Zimmermann O, Hansmann UHE. Simulation of Top7-CFr: A transient Helix Extension Guides Folding. Proc Natl Acad Sci (USA). 2008; 105:8004–7. [PubMed: 18408166]
7. Tuinstra RL, Peterson FC, Kutlesa S, Elgin ES, Kron MA, Volkman BF. Interconversion Between Two Unrelated Protein Folds in the Lymphotactin Native State. Proc Natl Acad Sci (USA). 2008; 105:5057–62. [PubMed: 18364395]
8. Sander IM, Chaney JL, Clark PL. Expanding Anfinsen's Principle: Contributions of Synonymous Codon Selection to Rational Protein Design. J Am Chem Soc. 2014; 136:858–61. [PubMed: 24392935]
9. Burmann BM, Knauer SH, Sevostyanova A, Schweimer K, Mooney RA, Landick R, Artsimovitch I, Roesch P. An Alpha Helix to Beta Barrel Domain Switch Transforms the Transcription Factor RfaH into a Translation Factor. Cell. 2012; 150:291–303. [PubMed: 22817892]
10. Tomar SK, Knauer SH, Nandymazumdar M, Rosch P, Artsimovitch I. Interdomain Contacts Control Folding of Transcription Factor RfaH. Nucleic Acids Res. 2013; 41:10077–85. [PubMed: 23990324]
11. Gc JB, Bhandari YR, Gerstman BS, Chapagain PP. Molecular Dynamics Investigations of the Alpha-Helix to Beta-Barrel Conformational Transformation in the RfaH Transcription Factor. J Phys Chem B. 2014; 118:5101–8. [PubMed: 24758259]
12. Li S, Xiong B, Xu Y, Lu T, Luo X, Luo C, Shen J, Chen K, Zheng M, Jiang H. Mechanism of the All-Alpha to All-Beta Conformational Transition of RfaH-CTD: Molecular Dynamics Simulation and Markov State Model. J Chem Theory Comput. 2014; 10:2255–64. [PubMed: 26580748]
13. Gc JB, Gerstman BS, Chapagain PP. The Role of the Interdomain Interactions on RfaH Dynamics and Conformational Transformation. J Phys Chem B. 2015; 119:12750–9. [PubMed: 26374226]
14. Balasco N, Barone D, Vitagliano L. Structural Conversion of the Transformer Protein RfaH: New Insights Derived From Protein Structure Prediction and Molecular Dynamics Simulations. J Biomol Struct Dyn. 2015; 33:2173–9. [PubMed: 25483894]
15. Geyer GJ, Thompson EA. Annealing Markov Chain Monte Carlo with Applications to Ancestral Inference. J Am Stat Assn. 1995; 90:909–20.
16. Hukushima K, Nemoto K. Exchange Monte Carlo Method and Application to Spin Glass Simulations. J Phys Soc (Japan). 1996; 65:1604–8.
17. Tesi MC, van Rensburg EJJ, Orlandini E, Whittington SG. Monte Carlo Study of the Interacting Self-avoiding Walk Model in Three Dimensions. J Stat Phys. 1996; 82:155–81.
18. Hansmann UHE. Parallel Tempering Algorithm for Conformational Studies of Biological Molecules. Chem Phys Lett. 1997; 281:140–50.

19. Sugita Y, Okamoto Y. Replica-exchange Molecular Dynamics Method for Protein Folding. Chem Phys Lett. 1999; 314:141–51.
20. Nadler W, Hansmann UHE. Generalized Ensemble and Tempering Simulations: A Unified View. Phys Rev E Stat Nonlin Soft Matter Phys. 2007; 75:026109. [PubMed: 17358396]
21. Yasar F, Bernhardt NA, Hansmann UHE. Replica-exchange-with-tunneling for Fast Exploration of Protein Landscapes. J Chem Phys. 2015; 143:224102. [PubMed: 26671353]
22. Fukunishi H, Watanabe O, Takada S. On the Hamiltonian Replica Exchange Method for Efficient Sampling of Biomolecular Systems: Application to Protein Structure Prediction. J Chem Phys. 2002; 116:9058–67.
23. Kwak W, Hansmann UHE. Efficient Sampling of Protein Structures by Model Hopping. Phys Rev Lett. 2005; 95:138102. [PubMed: 16197184]
24. Bernhardt NA, Xi W, Wang W, Hansmann UHE. Simulating Protein Fold Switching by Replica Exchange with Tunneling. J Chem Theory Comput. 2016; 12:5656–66. [PubMed: 27767301]
25. Zhang H, Xi W, Hansmann UHE, Wei Y. Fibril-Barrel Transitions in Cylindrin Amyloids. J Chem Theory Comput. 2017; 13:3936–44. [PubMed: 28671829]
26. Alexander PA, He Y, Chen Y, Orban J, Bryan PN. The Design and Characterization of Two Proteins With 88% Sequence Identity but Different Structure and Function. Proc Natl Acad Sci (USA). 2007; 104:11963–8. [PubMed: 17609385]
27. Alexander PA, He Y, Chen Y, Orban J, Bryan PN. A Minimal Sequence Code for Switching Protein Structure and Function. Proc Natl Acad Sci (USA). 2009; 106:21149–54. [PubMed: 19923431]
28. Bryan PN, Orban J. Proteins That Switch Folds. Curr Opin Struct Biol. 2010; 20:482–8. [PubMed: 20591649]
29. Lee J, Joo K, Brooks BR, Lee J. The Atomistic Mechanism of Conformational Transition of Adenylate Kinase Investigated by Lorentzian Structure-Based Potential. J Chem Theory Comput. 2015; 11(7):3211–24. [PubMed: 26575758]
30. Meinke JH, Hansmann UHE. Protein Simulations Combining an All-atom Force Field with a Go-Term. J Phys:Cond Mat. 2007; 19:285215.
31. Zhang W, Chen J. Accelerate Sampling in Atomistic Energy Landscapes Using Topology-Based Coarse-Grained Models. J Chem Theor Comp. 2014; 10:918–23.
32. Moritsugu K, Terada T, Kidera A. Scalable Free Energy Calculation of Proteins Via Multiscale Essential Sampling. J Chem Phys. 2010; 133:224105. [PubMed: 21171681]
33. Hess B, Kutzner C, van der Spoel D, Lindahl E. GROMACS 4: Algorithms for Highly Efficient, Load-balanced, and Scalable Molecular Simulation. J Chem Theory Comput. 2008; 4:435–47. [PubMed: 26620784]
34. Best RB, Zhu X, Shim J, Lopes PE, Mittal J, Feig M, Mackerell ADJ. Optimization of the Additive CHARMM All-atom Protein Force Field Targeting Improved Sampling of the Backbone Phi, Psi and Side-chain Chi(1) and Chi(2) Dihedral Angles. Chem Theory Comput. 2012; 8(9):3257–73.
35. Onufriev A, Bashford D, Case DA. Exploring Protein Native States and Large-scale Conformational Changes with a Modified Generalized Born Model. Proteins. 2004; 55:383–94. [PubMed: 15048829]
36. Whitford PC, Noel JK, Gosavi S, Schug A, Sanbonmatsu KY, Onuchic JN. An All-atom Structure-based Potential for Proteins: Bridging Minimal Models with All-atom Empirical Forcefields. Proteins. 2009; 75:430–41. [PubMed: 18837035]
37. Noel JK, Whitford PC, Sanbonmatsu KY, Onuchic JN. SMOG@ctbp: Simplified Deployment of Structure-based Models in GROMACS. Nucleic Acids Res. 2010; 38:W657–61. [PubMed: 20525782]
38. Hess B. P-LINCS: A Parallel Linear Constraint Solver for Molecular Simulation. J Chem Theory Comput. 2008; 4:116–122. [PubMed: 26619985]
39. Bussi G, Donadio D, Parrinello M. Canonical Sampling Through Velocity Rescaling. J Chem Phys. 2007; 126:014101. [PubMed: 17212484]
40. Daura X, Gademann K, Jaun B, Seebach D, Gunsteren W, Mark A. Peptide Folding: When Simulation Meets Experiment. Angew Chem Int Ed. 1999; 38:236–40.

41. Humphrey W, Dalke A, Schulten K. VMD: Visual Molecular Dynamics. J Mol Graph. 1996; 14:33–8. 27–8. [PubMed: 8744570]

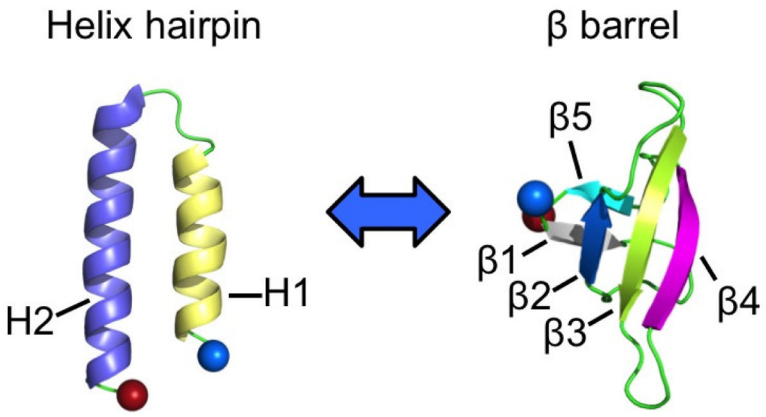

Figure 1.

The two folds observed for the C-terminal domain (RfaH-CTD) of the transcription factor RfaH. The N-terminus of RfaH-CTD is marked by a blue ball and the C-terminus a red ball.

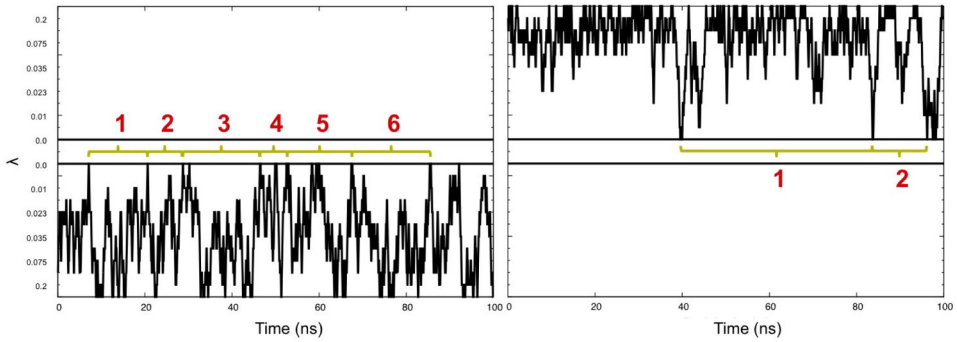

Figure 2.

Example of replica walking through λ space, from with a Go-model biasing toward the helix hairpin to a replica with λ = 0 (no bias) (left), and from λ = 0 toward replica with a Go-model biasing to the β-barrel (right). Tunneling events are numbered in red. Horizontal black lines mark the λ = 0 replica.

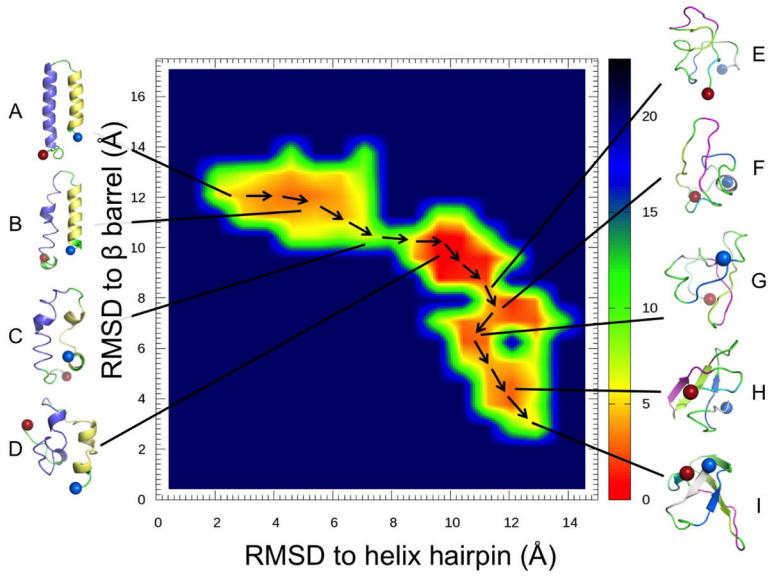

Figure 3.

Free energy landscape, in units of RT, of the switching protein RfaH-CTD projected on the root-mean-square deviation (RMSD) with respect to the helix hairpin structure of the protein and with respect to the protein in the β-barrel form. Representative configurations are shown for the main basins in the landscape.

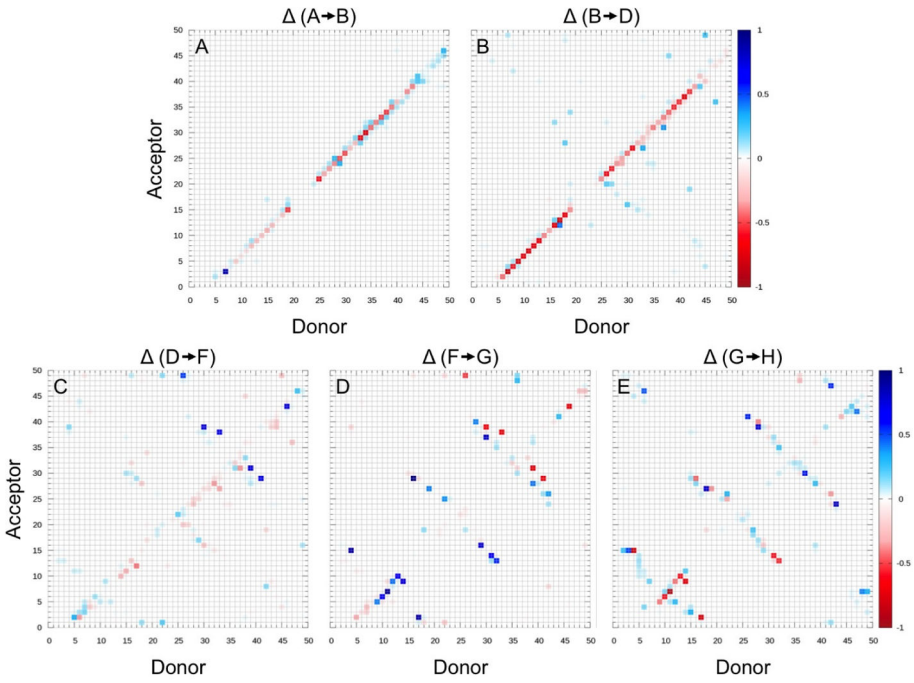

Figure 4.

Percentage of structures that gained (blue) or lost (red) backbone hydrogen bonds between the residues indicated on x and y axis, when converting from one region of the free energy landscape to another. The involved regions are indicated at the top of each panel, with the indices corresponding to the ones defined in Figure 3.

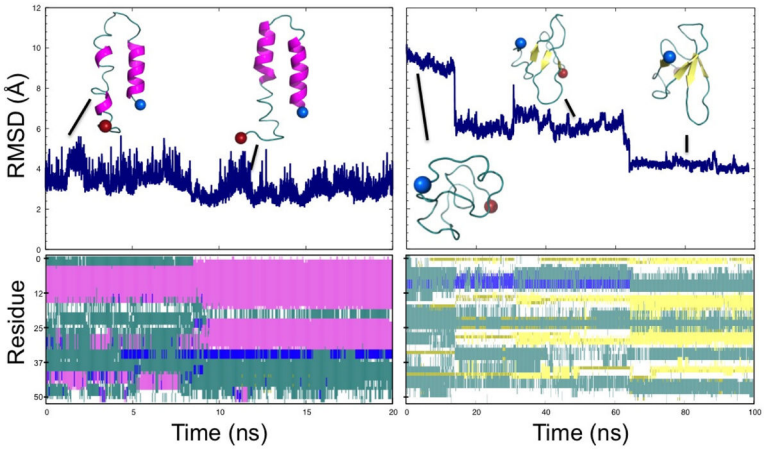

Figure 5.

Formation of the helix hairpin (left panels) and the β-barrel (right panels). Top panels show the root-mean-square-deviation (RMSD) to the helix hairpin (left) and the β-barrel (right). Configurations from various time points are shown. Secondary structure analysis by the VMD program[41] is shown in the bottom panel. Here, pink represents &*agr;* helices and yellow β-sheets.

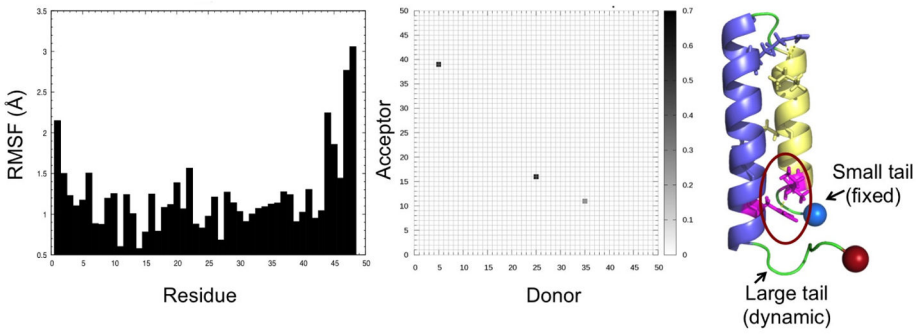

Figure 6.

Root-mean-square-fluctuation (RMSF) computed for configurations close to the the helix-hairpin state (less than 2.5 angstroms to the ideal fold) (left panel). Hydrogen bonding between helix 1 and helix 2 for these configurations (middle panel). The helix hairpin structure is shown in the right panel, with the tail segments labeled and the N-terminal tail stabilizing hydrogen bond circled in red.